Cell, Vol. 116, 565–576, February 20, 2004, Copyright ©2004 by Cell Press

Structure of the Human Transferrin Receptor-Transferrin Complex

Yifan Cheng,[1] Olga Zak,[2] Philip Aisen,[2] Stephen C. Harrison,[3,4] and Thomas Walz[1,*]
[1]Department of Cell Biology
Harvard Medical School
240 Longwood Avenue
Boston, Massachusetts 02115
[2]Department of Physiology and Biophysics
Albert Einstein College of Medicine
1300 Morris Park Avenue
Bronx, New York 10461
[3]Howard Hughes Medical Institute
and Children's Hospital Laboratory of
Molecular Medicine
320 Longwood Avenue
Boston, Massachusetts 02115
[4]Department of Biological Chemistry and
Molecular Pharmacology
Harvard Medical School
240 Longwood Avenue
Boston, Massachusetts 02115

Summary

Iron, insoluble as free Fe^{3+} and toxic as free Fe^{2+}, is distributed through the body as Fe^{3+} bound to transferrin (Tf) for delivery to cells by endocytosis of its complex with transferrin receptor (TfR). Although much is understood of the transferrin endocytotic cycle, little has been uncovered of the molecular details underlying the formation of the receptor-transferrin complex. Using cryo-electron microscopy, we have produced a density map of the TfR-Tf complex at subnanometer resolution. An atomic model, obtained by fitting crystal structures of diferric Tf and the receptor ectodomain into the map, shows that the Tf N-lobe is sandwiched between the membrane and the TfR ectodomain and that the C-lobe abuts the receptor helical domain. When Tf binds receptor, its N-lobe moves by about 9 Å with respect to its C-lobe. The structure of TfR-Tf complex helps account for known differences in the iron-release properties of free and receptor bound Tf.

Introduction

Many proteins depend on iron as a cofactor for redox reactions or ligand coordination. The facile conversion between ferrous (Fe^{2+}) and ferric iron (Fe^{3+}) poses significant dangers to living cells, however, as it can lead to the formation of hydroxyl radicals, a major source for oxidative damage to proteins, nucleic acids, and lipids. Moreover, under physiological conditions, ferric iron forms a highly insoluble hydroxide complex, so that despite its abundance, iron is not easily accessible to cells. Toxicity and insolubility have forced the evolution of highly sophisticated machineries for acquiring, storing, and distributing iron. In vertebrates, iron is transported in the serum bound to transferrin (Tf), which also delivers it to cells using an endocytotic pathway involving the transferrin receptor (TfR) (reviewed in Enns et al., 1996). At the slightly alkaline extracellular pH of 7.4, Tf can bind one or two ferric ions, and two iron-bearing Tf molecules can bind the dimeric TfR; iron-free transferrin is not recognized by TfR at this pH. The complex is endocytosed, and the acidic pH of the endosomal lumen induces a conformational change in Tf that accompanies iron release. The emptied Tf (apoTf) molecules remain tightly bound to TfR at endosomal pH, and as the complex is returned to the cell surface the extracellular pH leads to the dissociation of the apo-Tf molecules from the receptor.

Vertebrate Tf, a bilobed glycoprotein of 80 kDa, belongs to a family of homologous proteins (reviewed in Baker, 1994), most of which have closely related amino acid sequence and three-dimensional (3D) structures. The crystal structures of several members of the Tf family have been determined, revealing the properties that allow strong but reversible iron binding (reviewed in Baker et al., 2003). The Tf polypeptide chain is arranged in two homologous halves (~40% sequence identity), termed N- and C-lobe. Each lobe contains two domains (N_1, N_2 and C_1, C_2), connected by a flexible hinge. In the open, iron-free conformation, the two domains are well separated and form a large water-filled cleft for easy access by Fe^{3+}. Iron binding by Tf depends on a synergistic anion, usually carbonate. The carbonate ion, two Tyr, a His, and an Asp satisfy the coordination needs of Fe^{3+} to form a strong iron binding site in the closed conformation of Tf. Iron release is triggered by a drop in pH, which results first in protonation and dissociation of the synergistic anion, followed by protonation of His and/or Tyr ligands, and ultimately in release of the iron. For passage across the endosomal membrane via the iron transporter DMT1, iron must be reduced to the ferrous state; whether such reduction precedes or follows release from transferrin is not clear.

The best-characterized receptor for human Tf is the widely expressed TfR1 (reviewed in Enns et al., 1996). A homologous receptor (TfR2), predominantly expressed in the liver but of uncertain function, has also been described (Kawabata et al., 1999). Our present concern is with TfR1, or more simply TfR, a homodimeric type II transmembrane protein, with a small cytoplasmic domain, a single-pass transmembrane region, and a large extracellular domain. The crystal structure of the butterfly-shaped dimeric TfR ectodomain shows that each monomer has three structurally distinct domains: a protease-like domain proximal to the membrane, a helical domain accounting for all the dimer contacts, and a membrane-distal apical domain (Lawrence et al., 1999). A model for the TfR-Tf complex was proposed (Lawrence et al., 1999), based on the crystal structures of the TfR ectodomain and Tf, but no 3D crystals of any TfR-Tf complex have been obtained to test that proposal.

Iron release by Tf has been studied extensively

*Correspondence: twalz@hms.harvard.edu

(Kretchmar and Raymond, 1988; Egan et al., 1992; El Hage Chahine and Pakdaman, 1995; Halbrooks et al., 2003; Zak et al., 1997). TfR facilitates iron release from the C-lobe, probably by inducing a conformational change in Tf. Moreover, comparative studies of mono- and diferric Tf show that one lobe communicates its iron binding state to the other. The underlying mechanisms remain to be elucidated, but an α-helix at the C terminus of Tf, which lies in proximity to the N-lobe, is a plausible candidate to mediate interlobe communication (Jameson et al., 1998).

Iron homeostasis in vertebrate cells is regulated primarily at the stage of iron uptake, as most cells lack mechanisms for iron export. The main target for regulation of iron uptake is TfR (Aisen et al., 2001; Chan and Gerhardt, 1992; Chan et al., 1994; Crichton, 2001; Crichton et al., 2002; Rao et al., 1986; Richardson and Ponka, 1997). One mechanism works by control of TfR mRNA stability (Binder et al., 1994). Another involves HFE, the protein mutated in hereditary hemochromatosis (HH) (reviewed in Bomford, 2002). HFE is homologous to class I major-histocompatibility complex (MHC-I) proteins (Feder et al., 1997). Like MHC-I proteins, HFE must assemble with β2 microglobulin (β2m) to arrive at the cell surface, where it competes with Tf for binding to TfR (Lebron et al., 1999). The crystal structure of the HFE-β2m complex has been determined (Lebron et al., 1998), as has its complex with TfR (Bennett et al., 2000). The HFE binding site on TfR is on the helical domain, and mutational analysis of TfR shows that it overlaps with the binding site for Tf (West et al., 2001).

In this study, we have used cryo-electron microscopy (cryo-EM) and single particle averaging techniques to determine a density map for the human TfR-diferric Tf (dTf) complex at subnanometer resolution, an unusually high resolution for single-particle analysis. We can dock the crystal structures of the TfR and Tf molecules into our density map with high accuracy. The resulting model for the complex reveals an unexpected binding mode for dTf and TfR, shows a conformational change in Tf induced by association with TfR, and illustrates the overlap of HFE and Tf binding sites on TfR.

Results

Cryo-EM of the TfR-dTf Complex

Vitrification (Adrian et al., 1984), which preserves the specimen in a near-native environment, is the preferred technique for visualizing single protein complexes by EM. It overcomes the problems of limited resolution and molecular distortions associated with negative staining. The main drawback of vitrification is the poor signal-to-noise ratio (SNR) in images of ice-embedded specimens, posing severe difficulties when attempting to study small assemblies. The total mass of the TfR-dTf complex of about 290 kDa is small for the cryo-EM approach. We therefore took care to embed the specimen in a very thin ice layer to reduce background noise, and we used large defocus values, ranging from 3 to 5 μm, to increase phase contrast in the images. We also used a sample buffer of very low density. We rejected lower contrast images during processing (we assign the variability among different preparations to variations in thickness of the ice layer) and images that were affected by image drift. Figure 1A shows a typical raw image used for structure analysis, in which the individual particles are clearly visible.

We selected 36,266 particles from 196 images. To bring this number into perspective, our 36,000 particle images of the 2-fold symmetric TfR-dTf complex would correspond to 1200 images of a virus with icosahedral symmetry; 6400 particles were used to obtain the 7.4 Å resolution map of the icosahedral HBV capsid (Bottcher et al., 1997). The particle images were aligned and classified into 200 classes. Figure 1B shows a number of representative class averages and examples of corresponding raw images. Individual domains of the TfR-dTf complex are already clearly visible in the raw images, and they are merely enhanced in the class averages, indicating that the alignment and classification procedures have produced correct results. The resolution of a density map determined by single particle EM depends strongly on the precision with which individual particle images can be aligned to each other, which in turn depends on the size, symmetry, and shape of the particle. Although the TfR-dTf complex is small and only 2-fold symmetric, it has a very distinct shape. The spikiness of the complex probably aided alignment of particle images.

An initial 3D reconstruction of the TfR-dTf complex was obtained by the angular reconstitution approach (Van Heel, 1987) as implemented in the IMAGIC-V software (van Heel et al., 1996), imposing 2-fold symmetry. The orientational parameters (x, y, and the three Euler angles) were then refined and the contrast transfer function (CTF) corrected for each individual particle image, using the program FREALIGN (Grigorieff, 1998). As the resolution of a density map increases, accuracy of the CTF correction becomes more important. Image tilt leads to a gradual change in the defocus (and accordingly of the CTF) in a direction perpendicular to the tilt axis, and allowing for this change becomes especially important when using high defocus values to enhance image contrast. We therefore corrected carefully for image tilt (see Supplemental Data available at http://www.cell.com/cgi/content/full/116/4/565/DC1).

The Euler angle distribution of the 36,266 particles shows preferred orientations of the TfR-dTf complex in the ice layer, probably due to orientation on the air-water interface (Figure 1C). Nonetheless, the orientations of the particles fully cover Euler space, demonstrating that the views used in our reconstruction fully define the structure of the TfR-dTf complex.

The resolution of the final density map was assessed by Fourier shell correlation (FSC). According to the conservative resolution criterion, FSC = 0.5, the density map of the TfR-dTf complex has a nominal resolution of 7.5 Å (Figure 1D). The spectral signal-to-noise ratio (SSNR) criterion (Unser et al., 1987) yielded the same nominal resolution of 7.5 Å (data not shown). Moreover, the phase residual, which we used to follow the refinement of the density map by FREALIGN, was 39.8° in the resolution range from 7.7 Å to 7.5 Å, indicating meaningful information at this resolution (random phases are 90°). Thus, all resolution criteria are consistent. Figure 1E shows different views of the 2-fold symmetrized density map of the TfR-dTf complex filtered to a resolution of

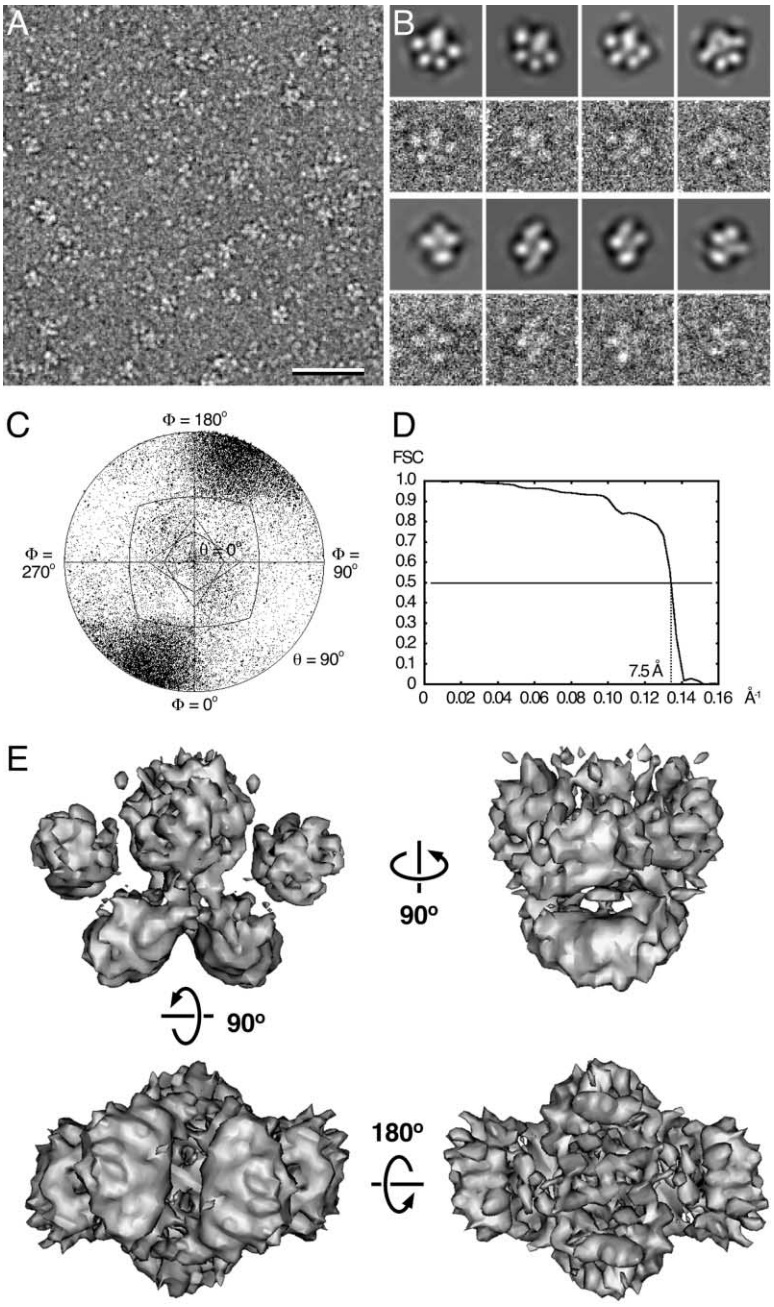

Figure 1. Single Particle Electron Microscopy of Human TfR-dTf Complex

(A) In low-dose images of TfR-Tf complexes embedded in a thin layer of vitrified ice, individual TfR-dTf complexes can be seen clearly. Many complexes show a large central density representing the receptor and four smaller peripheral densities representing the transferrin lobes. The contrast of the image was reversed and the scale bar corresponds to 50 nm.

(B) Raw images of individual TfR-dTf complexes (rows 2 and 4) are in good agreement with their corresponding class averages (rows 1 and 3). Side length is 27 nm.

(C) A plot of the angular distribution of the particles shows preferential orientations of the complexes in the ice layer, but data points are present in all areas of the Euler space, demonstrating that there are no missing views.

(D) The 0.5 criterion for the Fourier shell correlation resolution measure indicates a resolution of 7.5 Å for the final density map.

(E) The four views on the surface-rendered density map of the TfR-dTf complex show a wealth of fine structure, which made it possible to dock the crystal structures of the molecules accurately into the EM density map of the complex.

7.5 Å. A large central density represents TfR, and four peripheral densities correspond to the individual lobes of the two bilobal dTf molecules. The wealth of distinct fine structural detail enabled us to dock the crystal structures for TfR and dTf into the density map with high precision.

Achieving a density map at subnanometer resolution for the TfR-dTf complex by single particle EM has probably resulted from a number of favorable contributing factors. We believe that the large number of high-contrast particle images, the spiky shape of our subject, the use of a tilt-corrected CTF, and the use of FREALIGN for refining orientational parameters and for 3D reconstruction (Grigorieff, 1998) have all contributed. As Grigorieff (2000) has pointed out, however, refinement using large data sets such as ours can cause both the FSC and the SSNR to overestimate resolution. It is therefore important that a claimed nominal resolution be supported by clear density features. At 10 Å or better, α helices should be visible as rods. Individual helices in the TfR helical domain are very clearly resolved in our map, confirming the assessment of subnanometer resolution.

Docking the TfR and dTf Crystal Structures into the Electron Density Map

To build an atomic model of the TfR-dTf complex, we first fit the crystal structure of the TfR ectodomain (Lawrence et al., 1999) into the map. We then placed the structures for the Tf N-lobe (TfN) and the Tf C-lobe (TfC).

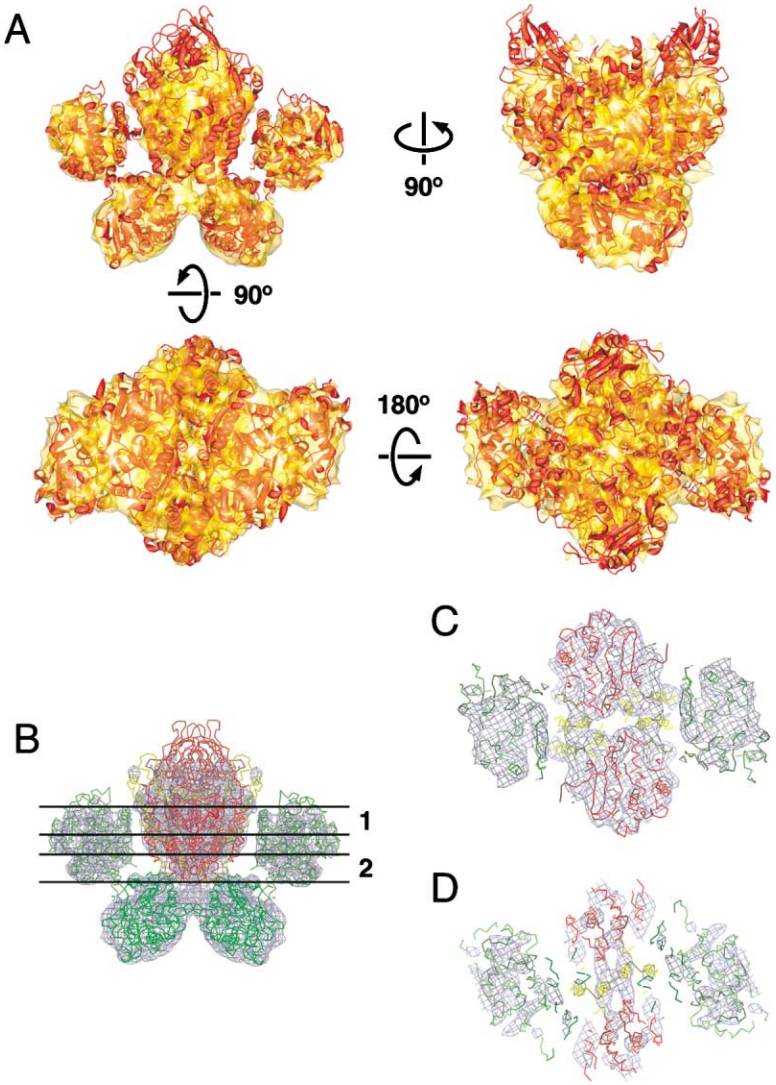

Figure 2. Fitting of the Crystal Structures for the TfR Ectodomain and dTf into the EM Density Map

(A) The same views as in Figure 1E reveal the good fit of the crystal structures (red) into the EM density map (gold).

(B, C, and D) Sections 1 and 2 in B indicate the positions of the sections through the TfR-dTf complex shown in (C) and (D). The crystal structures are color-coded (red: TfR protease-like and apical domain; yellow: TfR helical domain; green Tf). The section shown in (C) depicts a part of the structure with a good match between density map and crystal structures, whereas the section shown in (D) corresponds to an area with a slightly inferior match.

For the N-lobe, we used the crystal structure of iron-loaded human serum Tf (MacGillivray et al., 1998), and for the C-lobe we used the crystal structure of rabbit serum Tf, which has 78% sequence identity and 92% sequence similarity with human serum Tf (Hall et al., 2002). Rabbit Tf binds well to human TfR (S.C.H., unpublished data), and it serves as an iron donor for human cells (Lim et al., 1987).

Docking each atomic structure individually into the density map, followed by computational rigid body refinement, gave an excellent fit. Figure 2A shows the final fit of the crystal structures in the EM map. The correlation coefficient of our EM map with a 7.5 Å density map calculated from our atomic model is 0.66. Several rod-shaped densities in the EM map correspond well to α helices in the TfR and dTf molecules. For example, most helices of the TfR helical domain are represented by corresponding densities with the exception of the α3 helix, for which some density is missing (Figures 2C and 2D). The TfR protease-like domain crystal structure also corresponds well to features in the EM map, which resolves the N-terminal helix of this domain. Density for the TfR apical domains is low or absent in the EM map as contoured in Figure 2, where the threshold was chosen to emphasize resolved α helices. If the contouring threshold is lowered, the EM map reveals densities covering the apical domains of TfR (data not shown). The lower density level of the apical domain is probably due to its flexible connection with the remainder of the receptor. Indeed, the apical domains of the eight TfR ectodomains in the asymmetric unit of the 3D crystals are in slightly different positions with respect to the bulk of the receptor, with correspondingly large crystallographic B-factors (Lawrence et al., 1999).

While the TfR crystal structure was straightforward to fit into the EM map, the similarity of the two Tf lobes made it more difficult to distinguish TfN and TfC. The density for a Tf molecule in the EM map showed two globular domains with two lateral connections, and one of those was likely to represent the loop connecting the two Tf lobes. These constraints allow four possible orientations for fitting the TfC and the TfN crystal structures into the EM map. Only one orientation produced a good overall match between the EM density map and

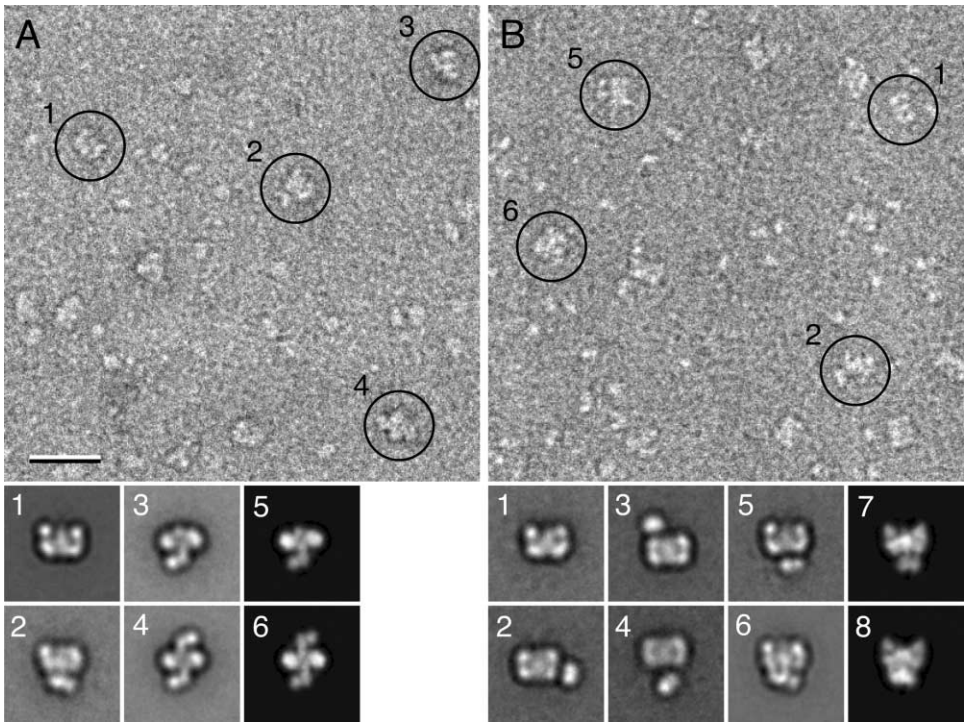

Figure 3. Complexes of the TfR Ectodomain with Isolated Tf C- and N-Lobes

(A) Micrograph area and projection averages of a negatively stained sample of TfR mixed with isolated C-lobe. The scale bar corresponds to 25 nm. 1: free TfR ectodomain (239 particles); 2: complex of C-lobe bound to the TfR binding site for the N-lobe (227 particles); 3 and 4: one and two C-lobe(s) bound to the receptor (485 and 544 particles); 5 and 6: projections produced from atomic models corresponding to the complexes shown in 3 and 4.

(B) Micrograph area and projection averages of a negatively stained sample of TfR mixed with isolated N-lobe. 1: free TfR ectodomain (870 particles); 2–4: TfR with unspecifically associated N-lobe (151, 184, and 105 particles); 5 and 6: one and two N-lobe(s) bound to the receptor (172 and 705 particles); 7 and 8: projections produced from atomic models corresponding to the complexes shown in 5 and 6. The projection averages illustrate that the C-lobe binds to its principal site (A3 and A4) but also to the specific N-lobe site (A2), while the N-lobe binds in specific fashion only to its own site (B5 and B6). Side length is 56 nm.

the atomic structure of Tf molecule. In this fitting, several rod-shaped densities in the EM map match well with α helices in the dTf molecule.

Comparison of the structure of bound Tf, obtained from independent dockings of N- and C-lobes as just described, with the structure of free rabbit diferric serum Tf (Hall et al., 2002) shows that the two lobes have shifted with respect to each other by about 9 Å (Figures 5C, 5D, and 5E). None of the crystal structures of diferric or apo-Tf molecules show this conformation, so we believe that the change is linked to receptor binding.

The C-terminal helix of Tf, residues 665–679 in the second half of domain C_1 is linked back to the first part of domain C_1 by a disulfide bond (residues Cys 674 and Cys 402) and also contacts the N-lobe. Although our fit of the C-lobe structure into the density map was excellent, density for the C-terminal helix was weak. We believe that the movement of the N-lobe relative to the C-lobe upon receptor binding may affect the structure of this C-terminal helix.

Binding of Isolated Tf-N and Tf-C Lobes to the TfR

To confirm the assignment of TfN and TfC, we examined complexes of isolated Tf N- and C-lobes with TfR, using negative-stain EM (Figures 3A and 3B). TfR-containing particles were selected from 20 electron micrographs of TfR-TfN and TfR-TfC, and the particle images were used to calculate class averages (Figure 3A, parts 1–4 and Figure 3B, parts 1–6). Some of the final classes appeared to correspond to complexes of TfR with one or two C-lobe(s) bound (Figure 3A, parts 3 and 4) or respectively, one or two N-lobe(s) bound (Figures 3B, parts 5 and 6). To confirm this interpretation, we created models for the four putative complexes (TfR-TfN, TfR-$(TfN)_2$, TfR-TfC, TfR-$(TfC)_2$) and calculated density maps filtered to a resolution of 25 Å. Projections calculated from the density maps at regular angular intervals were then compared to the corresponding class averages by crosscorrelation. This procedure identified projections from the density maps that correlated very well with the corresponding class averages (Figure 3A, parts 5 and 6 and Figure 3B, parts 7 and 8).

These results confirmed our assignment of the N- and C-lobes in the cryo-EM density map. In addition, the binding of isolated Tf lobes revealed distinct receptor binding characteristics for each of the two lobes. The N-lobe bound to its designated binding site on TfR (Figure 3B, parts 5 and 6), but also tended to associate with the receptor in nonspecific ways (Figure 3B, parts 2–4). While the C-lobe showed no tendency to interact with the receptor nonspecifically and bound predominantly

to its own binding site (Figure 3A, parts 3 and 4), it also bound frequently to the binding site for the N-lobe (compare Figure 3A, part 2 with Figure 3B, part 5). Due to the purity of the C-lobe preparation (Zak and Aisen, 2002), the lack of receptors with two lobes bound to the same side, and the relatively large number of "wrong" complexes, it is unlikely that the extra density on the receptor represents a contamination of N-lobe in our C-lobe preparation.

Molecular Anatomy of the TfR-dTf Complex

Our model based on the EM map (Figures 4A and 4B) reveals that dTf and TfR interact quite differently with each other than in the model proposed from the crystal structures alone (Lawrence et al., 1999). The C-lobe binds the helical domain of TfR, at a somewhat different position and in a quite different orientation than previously proposed, and the N-lobe extends toward the membrane, rather than away from it. The C-lobe thus interacts with the side of the receptor dimer, while the N-lobe inserts into the gap between the large TfR ectodomains and the membrane surface. The crystallized TfR ectodomain includes residues from 122 to the C terminus and lacks 33 residues known to form a stalk between the bulk of the ectodomain and the transmembrane segment (indicated by black lines in Figures 4A and 4C). An earlier cryo-EM study of TfR reconstituted into liposomes indicated that the TfR stalk spans a gap of about 30 Å between the ectodomain of TfR and the lipid bilayer (Fuchs et al., 1998). This gap is sufficient to accommodate the N-lobe (Figure 4A).

Figure 4B shows a view of the surface of the TfR-dTf complex that faces the membrane and Figure 4F shows the same view but with the N-lobe represented as a space-filling model. This representation of the complex reveals an elongated opening between the two N-lobes with dimensions of about 12 $\times$ 26 Å. The two stalks that connect the dimeric TfR ectodomain to the membrane are linked to each other by intermolecular disulfide bridges between residues Cys 89 and Cys 98 in the two receptor molecules (Jing and Trowbridge, 1987). We therefore propose that the stalks pass through the space between the two N-lobes of bound Tf.

TfR-dTf Contacts

The resolution of our map is not high enough to locate individual side chains, but the atomic model we have created based on the EM map and on the crystal structures of the components allows us to suggest which residues may be involved in interactions between dTf and TfR.

The two dTf lobes interact with TfR quite differently. The C-lobe and TfR approach each other over a single, continuous contact, where the C_1 domain forms a large interaction surface with α helices 1, 2, and 3 of the TfR helical domain (Figure 5A). The N-lobe and TfR are close to each other at two positions. The N_1 domain may interact with helices α3 and α4 of the TfR helical domain, which we will refer to as contact I, and the N_2 domain may interact with helix α1 of the TfR protease-like domain, referred to as contact II (Figure 5B). There may be a tenuous contact between the N_1 domain and the protease-like domain of the other TfR subunit in the dimer; this contact could become more extensive when the N-lobe opens up in releasing iron.

The residues in the helical domain of human TfR positioned close to the C-lobe and the residues in the dTf molecule in the immediate vicinity of TfR are enumerated in the caption to Figure 5. These residues of rabbit serum Tf are all conserved in human serum Tf with the exception of Glu369, which is substituted by a valine. Although detailed analysis of the interactions is not possible, four of the TfR residues are basic, while four (human) or five (rabbit) of the TfC residues are acidic. This arrangement suggests a network of salt bridges between a predominantly positively charged patch on TfR and a predominantly negatively charged patch on the C-lobe of Tf. Interactions of the N-lobe with TfR are probably more complex. In contact II, helix α1 of the protease-like domain of TfR seems to contribute three nonpolar residues and one acidic residue, while the interacting residues on the N_2 domain of Tf may include two prolines, two basic residues, and possibly an acidic residue (see caption to Figure 5). This arrangement suggests binding site II to be composed of hydrophobic and ionic interactions. Contact I is likewise a mixed interface.

Many of the TfR residues that we implicate in Tf binding have also been identified by mutational analysis of TfR (Giannetti et al., 2003) and hydroxyl-radical footprinting of the TfR-dTf complex (Liu et al., 2003). To provide corresponding data for the binding site in Tf, we have mutated to alanine three of the Tf residues at the interface in our structure: His349, Asp356, and Glu357. The binding of this triple Tf mutant to TfR-expressing K562 cells is reduced by a factor of 33 with respect to wild-type Tf (Figure 6A), and iron uptake by K562 cells is likewise reduced (Figure 6B).

Our experiments on binding of isolated Tf lobes and TfR show that the C-lobe can bind to the N-lobe site of TfR, as well as to the C-lobe site, but that the converse crossinteraction does not occur. We can explain these observations by modeling the respective interactions of the two closely related lobes with TfR. The models are consistent with observed specificities (see Supplemental Data available on *Cell*).

Model for the TfR-apoTf Complex

Crystal structures for the N-lobe of human apo-Tf (Jeffrey et al., 1998) and for the C-lobe of duck apo-ovotransferrin (Rawas et al., 1989) have been determined, enabling us to propose a model for the TfR-apoTf complex. To this end, we replaced the human ferric Tf N-lobe with the human apoTf N-lobe and the rabbit ferric Tf C-lobe with the duck apo-ovotransferrin C-lobe in a way that the interacting regions between Tf and TfR remained essentially unchanged. This procedure resulted in the model for the TfR-apoTf complex shown in Figures 4C and 4D. We note, however, that a recent mutational study indicates that dTf and apoTf may bind to slightly different positions on TfR (Giannetti et al., 2003). Therefore it will be necessary to determine the structure of the TfR-apoTf complex to understand fully this interaction and the opening of the Tf lobes; such work is in progress.

Iron Release from the N-lobe of Monoferric Tf

Earlier studies have found little difference in the iron release from the N-lobe between free and receptor

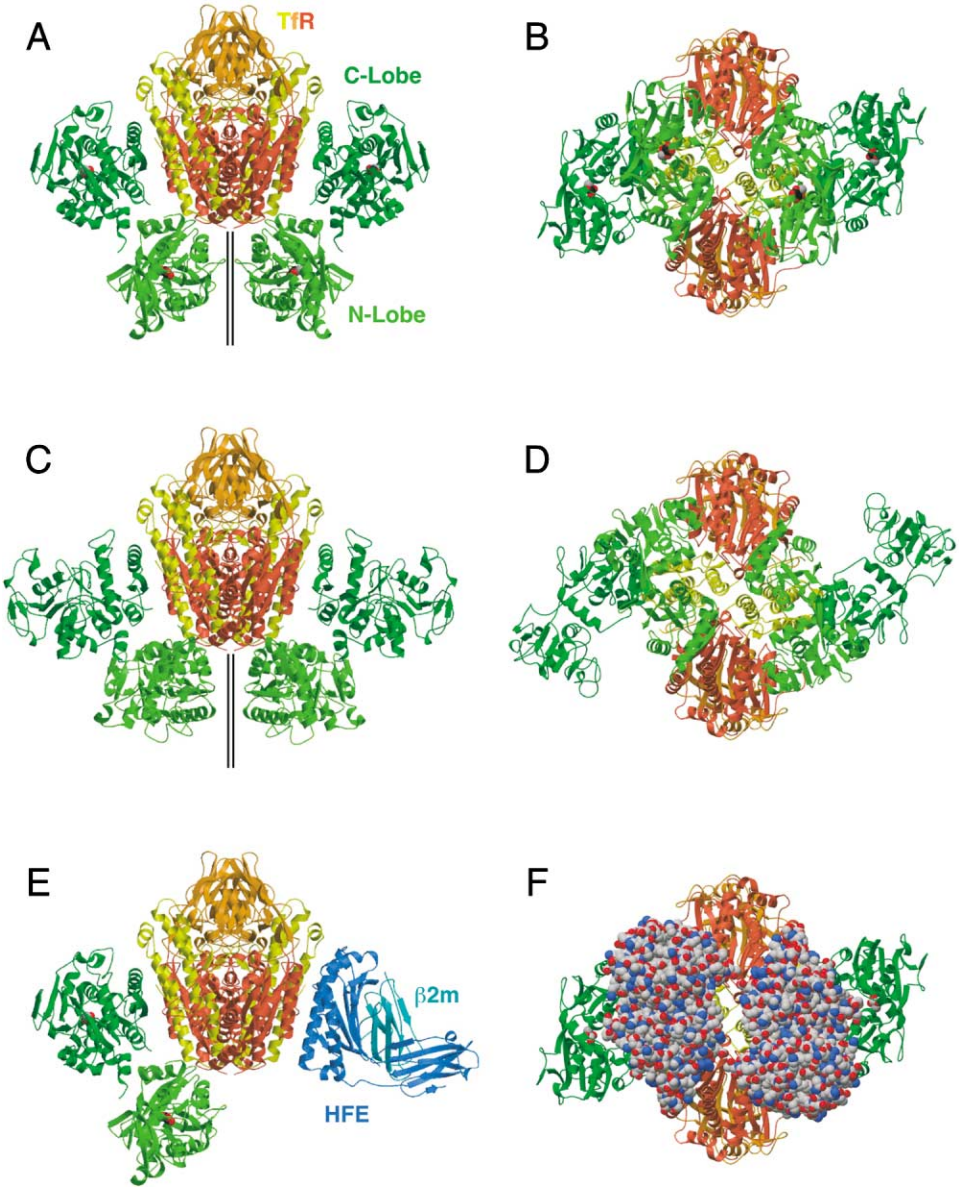

Figure 4. Atomic Model of the TfR-dTf Complex, Modeled Structure of the TfR-apoTf Complex, and Interactions of TfR with HFE and the Tf N-Lobe

(A) Face-on view and (B) bottom view on the atomic model of the TfR-dTf complex.

(C and D) The same views as in (A) and (B) on the modeled structure of the TfR-apoTf complex, in which Tf remains bound to TfR after iron release.

(E) Modeled structure of a ternary complex of the TfR dimer with one HFE and one Tf molecule bound.

(F) Same view as in (B) on the atomic model of the TfR-dTf complex with the two N-lobes in a space-filled representation to reveal the gap that provides sufficient space to accommodate the two TfR stalk domains. The figures are color-coded: red: TfR protease-like domain; yellow: TfR helical domain; orange: TfR apical domain; dark green: Tf C-lobe; light green: Tf N-lobe; dark blue: HFE; and light blue: β2 microglobulin. The TfR stalks are indicated by black lines in (A) and (C).

bound monoferric Tf (Bali and Aisen, 1991), but the contacts between the N-lobe and TfR, which involve both the N_1 and the N_2 domains, suggest that receptor binding should hamper N-lobe iron release. This observation has led us to revisit kinetics of iron release from the N-lobe of monoferric Tf. Indeed, at pH 7.4 the rate constant for iron release (1.04×10^{-3} s^{-1} for free monoferric Tf) drops by a factor of 4 (to 0.26×10^{-3} s^{-1}) upon receptor binding (Figure 6C). A 4-fold faster release rate in free Fe_N-Tf than in the Fe_N-Tf/TfR complex indicates that binding to receptor substantially impedes iron release from the N-lobe.

Discussion

Significance of the TfR-dTf Complex Structure

Uptake of Tf bound iron by TfR is one of the most intensely analyzed of the endocytic pathways. It serves as marker in many studies of clathrin-mediated endocytosis. There are, moreover, efforts to exploit this path-

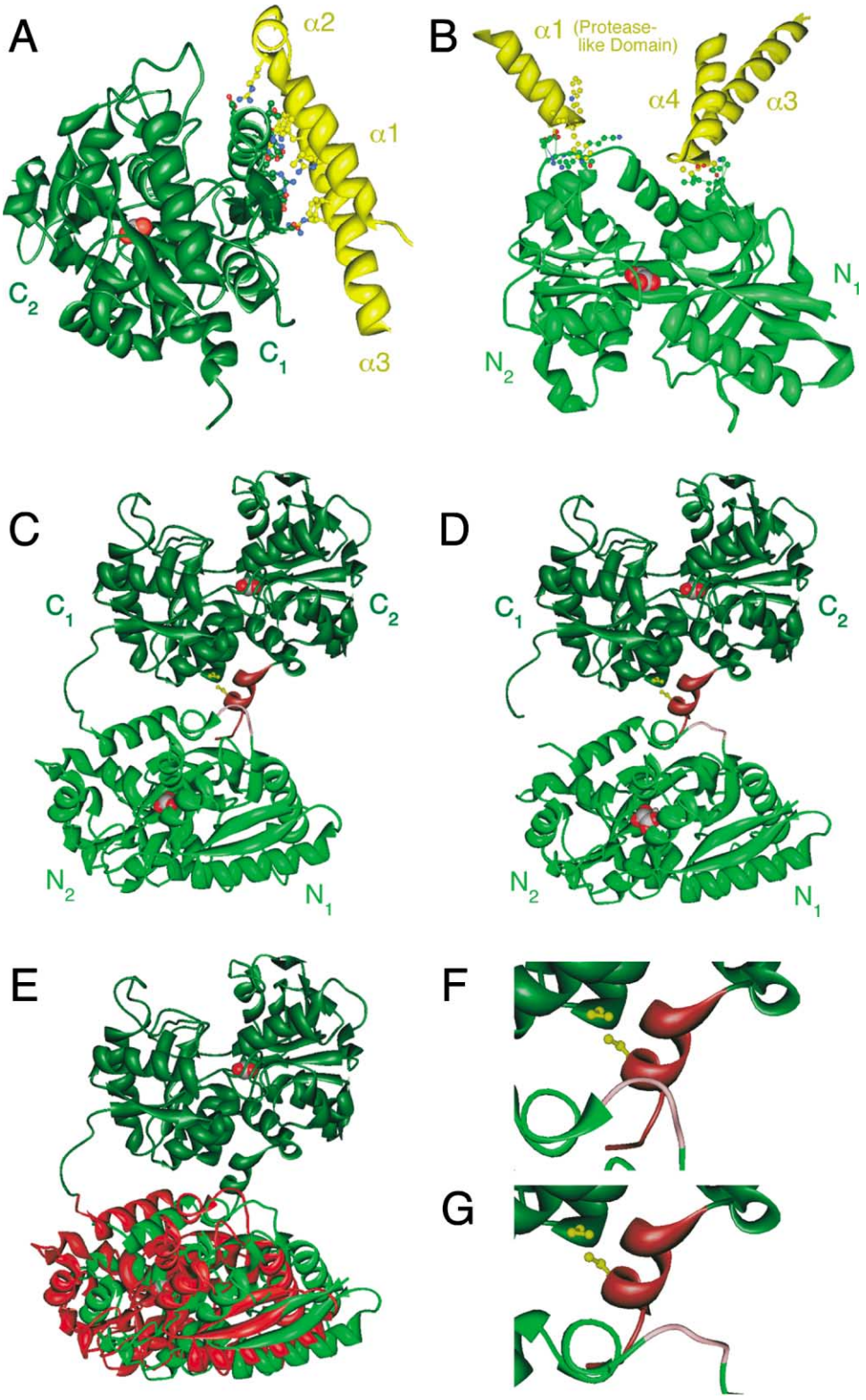

Figure 5. Interactions of Tf C- and N-Lobe with the TfR Ectodomain and Comparison of Bound Versus Free Tf

(A) Interaction of Tf C-lobe with the TfR ectodomain highlighting the side chains of the residues likely to be involved in the binding interaction. The residues in the helical domain of the TfR positioned close to the C-lobe are Leu619, Arg623 of helix α1, Arg629 of helix α2, and Gln640, Try643, Arg646, Phe650 and Arg651 of helix α3. The residues in the C-lobe positioned close to the helical domain of TfR are His349, Arg352, Leu353, Asp356, Glu357, Ser359, Val360, Glu367, Glu369, Ser370, and Glu372. The side chain noncarbon atoms of these residues are colored according to atom types. The side chain carbon atoms of Tf C-lobe are colored in green and those of TfR in yellow.

way for specific delivery of antitumor agents to rapidly proliferating cells (reviewed in Qian et al., 2002) as well as efforts to design tridentate iron chelators for the treatment of cancer and other diseases (reviewed in Nick et al., 2003). For all these applications, the structure of the TfR-dTf complex now permits site-directed modifications of the interacting proteins.

The most striking aspect of the TfR-dTf complex is the position of the transferrins. Rather than associating with the membrane-distal surfaces of the receptor (as considered in a previous model by Lawrence et al., 1999), the dTf molecules bind laterally to the dimeric TfR ectodomain and extend into the gap between the bulk of the receptor ectodomain and the membrane. The C-lobe of each Tf makes extensive contact with the helical domain of one of the receptors, and the N-lobe binds "beneath" the receptor, making contact with the protease-like and helical domains of the same subunit as the C-lobe. The N-lobe is thus sandwiched between the membrane and the TfR ectodomain. Binding of Tf to the "bottom" rather than to the "top" of TfR provides a structural precedent for this unanticipated mode of ligand-receptor interaction.

Between the N-lobes of the two receptor bound Tf molecules is a gap (Figure 4F), through which must pass the stalks of the TfR dimer as they connect the transmembrane segments to the globular ectodomains. With the possible exception of the restricted N-lobe interaction mentioned above, these contacts of N-lobes and stalks are the only positions at which one Tf molecule interacts with both subunits of TfR. The presence of the TfR stalks is unlikely to change the way in which Tf binds TfR, but it may influence the strength of the interaction, a hypothesis that awaits experimental tests. Of more general interest, the TfR-Tf example shows that extended stalk regions, present in many cell-surface proteins (e.g., CD8; Moody et al., 2001; Wong et al., 2003) can be more than just flexible linkers and can form integral structural elements in receptor-ligand complexes.

While our TfR-dTf structure now implicates the TfR stalks in the binding interaction, it also shows that the TfR apical domains do not participate in this interaction, leaving them without obvious function. A possible role for the apical domains might be to provide contact surfaces for the TfR-dTf complex to interact with other proteins. Candidates would be the postulated ferrireductase, required to reduce the iron before it can be exported from the endosome by the iron transporter DMT1, or even DMT1 itself (Gunshin et al., 1997).

The TfR-dTf Interface

Several approaches have yielded indirect information concerning the TfR-dTf interface. A study exploiting the observation that human Tf does not bind to chicken TfR used chimeric human/chicken TfRs to map the binding site for Tf to the C-terminal helical domain of TfR (residues 607–760) (Buchegger et al., 1996). Another mutational study also implicated this TfR region in Tf binding and identified a critical Arg-Gly-Asp motif in TfR (residues 646–648) (Dubljevic et al., 1999). Recently, an exhaustive mutational analysis of TfR (Giannetti et al., 2003) and an X-ray hydroxyl radical footprinting study (Liu et al., 2003) identified further residues involved in Tf binding. All these findings agree with the binding sites revealed by our density map.

Six of the TfR residues we identified in the C-lobe contact have been found to be important for Tf binding in the recent mutational analysis of TfR (Giannetti et al., 2003). These include the Arg of the previously implicated Arg-Gly-Asp motif. The large extent of the interacting surfaces suggests a strong association, in good agreement with experiments that identified the C-lobe as the primary contact of Tf and TfR (Zak et al., 1994). Because dTf only interacts with TfR through its C_1 domain (Figure 5A), leaving the C_2 domain free to move, binding to TfR places no constraints on the opening of the C-lobe and iron release.

In contrast to the C-lobe, the N-lobe makes two very localized contacts with TfR. The N_1 domain interacts with the helical domain; the N_2 domain with the protease-like domain (Figure 5B). Because the N-lobe interacts more weakly with TfR than does the C-lobe, mutation of TfR has identified only one residue involved in binding, Tyr 123 in the protease-like domain (Giannetti et al., 2003). We indeed find this residue at the interface with the N_2 domain. Our images of the isolated lobes bound to TfR are consistent with the weaker binding of the N-lobe. Isolated C-lobe binds the N-lobe site as well as the C-lobe site (although more weakly), but we do not see the additional nonspecific decoration of TfR that we find with N-lobe. One of the binding sites of the N-lobe is a hydrophobic patch, which might make it nonspecifically "sticky". The specific interaction is sufficiently weak that it went undetected in previous studies (Zak et al., 1994). The binding of both of its domains by TfR together with the loop connecting the two domains must clearly constrain the opening of the N-lobe. Because TfR binds laterally to the main opening motion of the lobe, these constraints may not be too severe. Monofer-

(B) Interaction of Tf N-lobe with the TfR ectodomain. The TfR residues likely to be involved in the binding interactions are Leu122, Tyr123, Trp124, and Asp125 of the protease-like domain and Asn662 and Glu664 of the helical domain. The residues in the N-lobe positioned close to TfR are Pro142, Arg143, Lys144, and Pro145 of the N_2 domain, and Tyr71, Leu72, Ala73, and Pro74 of the N_1 domain. The color-coding is the same as in (A).

(C) Crystal structure of rabbit serum Tf (Hall et al., 2002). The C-lobe is shown in dark green; the N-lobe, in light green; the C-terminal helix (residues 665–679), in red, and the interacting loop of the N-lobe (residues 306–309), in pink. Cys402 and Cys671, which form a disulfide bridge fixing the orientation of the C-terminal helix, are shown in yellow.

(D) Atomic model of Tf when bound to TfR as obtained by fitting the two lobes individually into the EM density map. The C-lobe is in the same orientation as in (C). The color-coding is the same as in (C).

(E) The shift between the Tf C- and the N-lobe that occurs upon receptor binding is best seen in a superposition of the two structures. When the orientation of the C-lobe (dark green) is kept constant, the N-lobe moves parallel to the C-lobe by a distance of about 9 Å from its original position in free Tf (red) to its position in the complex with the receptor (light green).

(F) Close-up of the interaction between the C-terminal helix and residues 306–309 in the N-lobe in free Tf.

(G) The interaction seen in free Tf (F) is not present in TfR bound Tf. Maintaining the interaction in TfR bound Tf would cause strain in the C-lobe and may help facilitate iron release from the C-lobe in receptor bound Tf. The color-coding in (F) and (G) is the same as in (C) and (D).

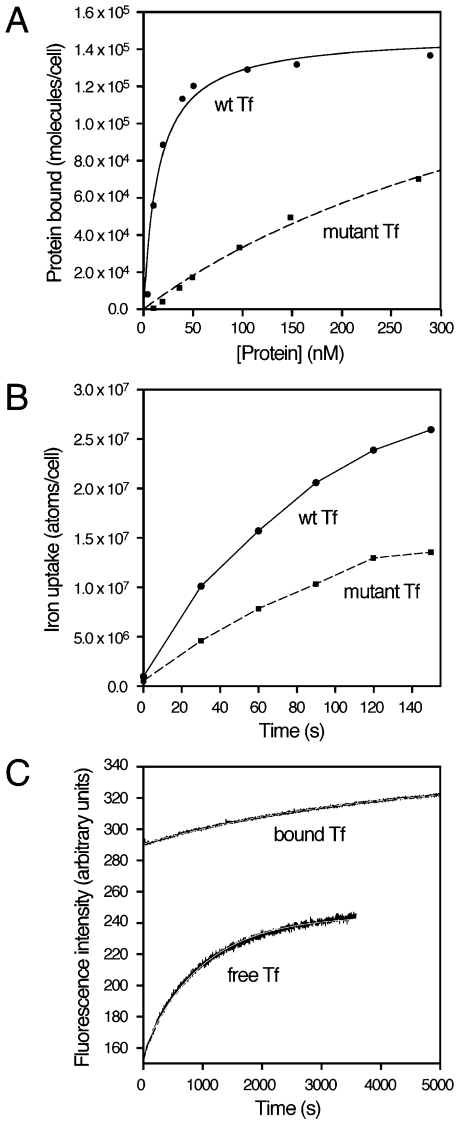

Figure 6. Receptor Binding and Iron Delivery of the Tf H349A-D356A-E357A Triple Mutant and Iron Release from the N-Lobe from Free and Receptor Bound Monoferric Tf

(A) Binding of wild-type Tf (solid line) and the Tf mutant H349A-D356A-E357A (dashed line) to K562 cells at 4°C. Binding isotherms have been corrected for nonspecific binding (i.e., binding not suppressed by a 100-fold excess of unlabeled protein). The binding constant drops by a factor of 33 from 6.7×10^7 M^{-1} for wild-type Tf to 2.0×10^6 M^{-1} for the triple mutant.

(B) Uptake of ^{59}Fe by K562 cells at 37°C from wild-type Tf (solid line) and Tf mutant H349A-D356A-E357A (dashed line), each at a concentration of 2.9×10^{-7} M. The calculated saturation of binding sites, determined from the binding isotherms, is 95% for the wild-type protein and 37% for the mutant. Binding and iron uptake studies were carried out as described in Zak and Aisen, 2002.

(C) Spectrofluorometric progress of iron release from free monoferric Tf N-lobe (lower curve) and from monoferric Tf N-lobe complexed to TfR ectodomain (upper curve) at pH 7.4 (0.05 M HEPES/0.1 M NaCl/0.1 M pyrophosphate). The release rate calculated by curve fitting drops by a factor of 4 from 1.04×10^{-3} s^{-1} for free monoferric Tf to 2.6×10^{-4} s^{-1} for receptor bound monoferric Tf.

ric Tf with iron bound to its N-lobe can still release iron, even when bound to TfR ectodomain, although less efficiently than does free Tf (Figure 6C). The TfR stalks could, of course, exert additional effects on Tf bound to intact receptor, as the stalks are likely to make further interactions with the N-lobe.

HFE competes with Tf for binding to TfR (Lebron et al., 1999). Comparison of our model with the crystal structure of the TfR-HFE complex (Bennett et al., 2000) shows how. A dimeric TfR can easily accommodate one HFE and one Tf molecule on opposite sides (Figure 4E), but binding of both molecules to the same side would cause severe steric clashes.

Conformational Changes in Tf

Upon receptor binding, the relative position of the two Tf lobes changes by about 9 Å, and the shift is in a direction normal to the long axis of the protein, resulting in a straightening of the molecule. If we dock the entire rabbit serum Tf molecule into the EM map as a single rigid body, we do not obtain a good fit. We therefore believe that the difference in the relative position of the two lobes is indeed an effect of the binding of Tf with its receptor, rather than an artifact of how we docked the structures of the two lobes or of our use of Tf-lobe structures from different species. The straightening of Tf upon receptor binding may well be communicated between the two Tf lobes by the C-terminal helix of the C-lobe. This helix is positioned at the interface between the two Tf lobes and has previously been implicated in interlobe communications (Jameson et al., 1998). The C-lobe, which binds TfR on its own with relatively high affinity, may associate first with the receptor, bringing the more weakly binding N-lobe into range of its site. A shift in the N-lobe would then allow it to be captured and held in place on the TfR surface. Upon release of Tf from the receptor, the N-lobe would slide back into its original position, which would be communicated again between the two lobes by the C-terminal helix.

Iron Release

When iron is released, the jaws of the C-lobe move approximately parallel to the membrane, as illustrated in Figures 4B and 4D. The position of the iron in the C-lobe is about 57 Å above the membrane surface (Figure 4A). Opening of the C-lobe can thus provide convenient access for other proteins, for example a ferrireductase, to accept iron after its release. This direct hand-off would limit the exposure of Fe^{3+} to hydrolysis. Consistent with this picture, receptor bound diferric Tf releases iron preferentially from the C-lobe at low pH (Bali and Aisen, 1991), thus helping to explain the predominance of iron in the N-lobe of circulating transferrin. The opening of the N-lobe is directed toward the membrane (Figures 4B and 4D), so that iron released from the N-lobe would have to diffuse "out from under" the TfR-Tf complex.

Iron release from the C-lobe is facilitated by binding of Tf to its receptor (Bali et al., 1991). The two Tf lobes are connected by a linker between the two lobes and the C-terminal helix (highlighted in red in Figures 5C, 5D, 5F, and 5G), which interacts with a loop in the N1 subdomain (highlighted in pink in Figures 5C, 5D, 5F,

and 5G). We suggest that strain induced in the C-lobe by displacement of the N-lobe, communicated by the linker connecting the two lobes and the interaction of the C-terminal helix with the N1 subdomain, may be part of the facilitating mechanism. The C-terminal helix has also been implicated in communicating the iron binding state of one lobe to the other (Jameson et al., 1998).

The Roles of the N- and C-Lobes in Iron Transport

The C-lobe by itself is effective in delivering iron to cells, but the isolated N-lobe is not (Zak et al., 1994; Zak and Aisen, 2002). Our structure for the TfR-dTf complex shows that binding of the C-lobe to the receptor imposes no new constraints on the opening of the C-lobe (Figures 4B and 4D), as only the C_1 domain interacts with the receptor, leaving the C_2 domain free to move. On binding to receptor, straightening of the Tf molecule may impart strain through the C-terminal helix and facilitate iron release from the C-lobe. The opening of the N-lobe is directed toward the membrane, probably impeding iron release and limiting accessibility to iron-accepting molecules. We also expect that binding to TfR will hinder N-lobe opening, because there is a TfR contact in each of its domains and because the N-lobe probably contacts the receptor stalks (Figures 4B and 4D). The data presented in Figure 6C are consistent with hindered N-lobe opening and with the observed switch of preferred iron release from the N-lobe in free Tf to the C-lobe in receptor bound Tf. A major role of the N-lobe in iron transport may therefore be in strengthening the interaction with TfR and in modulating iron release from the C-lobe (Zak and Aisen, 2003).

Experimental Procedures

Protein Preparation

Recombinant human TfR ectodomain containing residues 122 to 760 was expressed in CHO cells and purified as described (Lawrence et al., 1999). Nonglycosylated full-length Tf, in which the two native glycosylation sites at Asn 413 and Asn 611 have been ablated by mutation to Asp, was prepared as described for other Tf mutants (Zak et al., 1997). Isolated Tf N- and C-lobes were prepared as described (Mason et al., 1991; Zak and Aisen, 2002). The TfR-dTf complex was prepared by adding a 2-fold excess of dTf to TfR ectodomain and subsequent purification of the complex by gel-filtration chromatography. TfR-TfN and TfR-TfC complexes were prepared by adding a 5-fold molar excess of TfN or TfC to the TfR ectodomain without further purification. All complexes were prepared in 10 mM HEPES buffer, [pH 7.4], containing 100 mM NaCl and 0.05% NaN_3.

Electron Microscopy and Image Processing

Technical details concerning electron microscopy, image processing and docking of the crystal structures into the density map are provided in Supplemental Data (available on *Cell* website).

Iron Release from the N-lobe of Monoferric Transferrin

Monoferric transferrin loaded in the N-lobe was prepared by the method of Baldwin and de Sousa (1981) and verified by urea gel electrophoresis. Its complex with TfR was obtained by incubating a 2-fold molar excess of Fe_N-Tf with receptor in 50 mM HEPES/100 mM NaCl, [pH 7.4], for 2 hr at 37°C, then overnight in the cold. Size exclusion chromatography in the same buffer, using the Pharmacia Äkta Explorer 10 system, separated the complex from its unassociated components. Iron release at pH 7.4 (0.05 M HEPES/0.1 M NaCl/0.1 M pyrophosphate), from Fe_N-Tf, free and complexed to TfR, was measured at 25°C in duplicate by a previously described spectrofluorometric method (Zak and Aisen, 2002) with a sensitivity enhanced Photo Technology International instrument. Entry slits were set at 0.25 mm (1.0 nm resolution) to minimize photobleaching. Variations from means were less than ± 5%.

Acknowledgments

We thank Marina Babyonyshev for preparing TfR ectodomain and Mykol Larvie for preparing the TfR-dTf complex. We are endebted to Nikolaus Grigorieff for advice and help with the image processing. The EM facility at Harvard Medical School was established by a donation from the Giovanni Armenise Harvard Center for Structural Biology. This work was supported by NIH grant GM62580 (to T.W. and S.C.H.) and by DK15056 (to P.A.). S.C.H. is an Investigator in the Howard Hughes Medical Institute.

Received: September 11, 2003
Revised: December 15, 2003
Accepted: January 7, 2004
Published: February 19, 2004

References

Adrian, M., Dubochet, J., Lepault, J., and McDowall, A.W. (1984). Cryo-electron microscopy of viruses. Nature *308*, 32–36.

Aisen, P., Enns, C., and Wessling-Resnick, M. (2001). Chemistry and biology of eukaryotic iron metabolism. Int. J. Biochem. Cell Biol. *33*, 940–959.

Baker, E.N. (1994). Structure and reactivity of transferrins. Adv. Inorg. Chem. *41*, 389–463.

Baker, H.M., Anderson, B.F., and Naker, E.N. (2003). Dealing with iron: common structural principles in proteins that transport iron and heme. Proc. Natl. Acad. Sci. USA *100*, 3579–3583.

Baldwin, D.A., and de Sousa, D.M.R. (1981). The effect of salts on the kinetics of iron release from N-terminal and C-terminal monoferrictransferrins. Biochem. Biophys. Res. Commun. *99*, 1101–1107.

Bali, P.K., and Aisen, P. (1991). Receptor-modulated iron release from transferrin: differential effects on N- and C-terminal sites. Biochemistry *30*, 9947–9952.

Bali, P.K., Zak, O., and Aisen, P. (1991). A new role for the transferrin receptor in the release of iron from transferrin. Biochemistry *30*, 324–328.

Bennett, M.J., Lebron, J.A., and Bjorkman, P.J. (2000). Crystal structure of the hereditary haemochromatosis protein HFE complexed with transferrin receptor. Nature *403*, 46–53.

Binder, R., Horowitz, J.A., Basilion, J.P., Koeller, D.M., Klausser, R.D., and Harford, J.B. (1994). Evidence that the pathway of transferrin receptor in RNA degradation involves an endonucleolytic cleavage within the 3′-UTR and does not involve poly (A) tail shortening. EMBO J. *13*, 1969–1980.

Bomford, A. (2002). Genetics of haemochromatosis. Lancet *360*, 1673–1681.

Bottcher, B., Wynne, S.A., and Crowther, R.A. (1997). Determination of the fold of the core protein of hepatitis B virus by electron cryomicroscopy. Nature *386*, 88–91.

Buchegger, F., Trowbridge, I.S., Liu, L.F., White, S., and Collawn, J.F. (1996). Functional analysis of human/chicken transferrin receptor chimeras indicates that the carboxy-terminal region is important for ligand binding. Eur. J. Biochem. *235*, 9–17.

Chan, L.-N.L., and Gerhardt, E.M. (1992). Transferrin receptor gene is hyperexpressed and transcriptionally regulated in differentiating erythroid cells. J. Biol. Chem. *267*, 8254–8259.

Chan, R.Y., Seiser, C., Schulman, H.M., Kuhn, L.C., and Ponka, P. (1994). Regulation of transferrin receptor mRNA expression. Distinct regulatory features in erythroid cells. Eur. J. Biochem. *220*, 683–692.

Crichton, R.R. (2001). Inorganic Biochemistry of Iron Metabolism: From Molecular Mechanisms to Clinical Consequences. (New York: John Wiley & Sons).

Crichton, R.R., Wilmet, S., Legssyer, R., and Ward, R.J. (2002). Molecular and cellular mechanisms of iron homeostasis and toxicity in mammalian cells. J. Inorg. Biochem. *91*, 9–18.

Dubljevic, V., Sali, A., and Goding, J.W. (1999). A conserved RGD (Arg-Gly-Asp) motif in the transferrin receptor is required for binding to transferrin. Biochem. J. *341*, 11–14.

Egan, T.J., Ross, D.C., Purves, L.R., and Adams, P.A. (1992). Mechanism of iron release from human serum C-terminal monoferric transferrin to pyrophosphate: kinetic discrimination between alternative mechanisms. Inorg. Chem. *31*, 1994–1998.

El Hage Chahine, J.M., and Pakdaman, R. (1995). Transferrin, a mechanism for iron release. Eur. J. Biochem. *230*, 1102–1110.

Enns, C.A., Rutledge, E.A., and Williams, A.M. (1996). The transferrin receptor. Biomembranes *4*, 255–287.

Feder, J.N., Tsuchihashi, Z., Irrinki, A., Lee, V.K., Mapa, F.A., Morikang, E., Prass, C.E., Starnes, S.M., Wolff, R.K., Parkkila, S., et al. (1997). The hemochromatosis founder mutation in HLA-H disrupts b_2-microglobulin interaction and cell surface expression. J. Biol. Chem. *272*, 14025–14028.

Fuchs, H., Lucken, U., Tauber, R., Engel, A., and Gessner, R. (1998). Structural model of phospholipid-reconstituted human transferrin receptor derived by electron microscopy. Structure *6*, 1235–1243.

Giannetti, A.M., Snow, P.M., Zak, O., and Bjorkman, P.J. (2003). Mechanism for Multiple Ligand Recognition by Human Transferrin Receptor 1. PLoS Biol. E51.

Grigorieff, N. (1998). Three-dimensional structure of bovine NADH:ubiquinone oxidoreductase (complex I) at 22 Å in ice. J. Mol. Biol. *277*, 1033–1046.

Grigorieff, N. (2000). Resolution measurement in structures derived from single particles. Acta Crystallogr. *D56*, 1270–1277.

Gunshin, H., Mackenzie, B., Berger, U.V., Gunshin, Y., Romero, M.F., Boron, W.F., Nussberger, S., Gollan, J.L., and Hediger, M.A. (1997). Cloning and characterization of a mammalian proton-coupled metal-ion transporter. Nature *388*, 482–488.

Halbrooks, P.J., He, Q.Y., Briggs, S.K., Everse, S.J., Smith, V.C., MacGillivray, R.T.A., and Mason, A.B. (2003). Investigation of the mechanism of iron release from the C-lobe of human serum transferrin: mutational analysis of the role of a pH sensitive triad. Biochemistry *42*, 3701–3707.

Hall, D.R., Hadden, J.M., Leonard, G.A., Bailey, S., Neu, M., Winn, M., and Lindley, P.F. (2002). The crystal and molecular structures of diferric porcine and rabbit serum transferrins at resolutions of 2.15 and 2.60 Å, respectively. Acta Crystallogr. *D58*, 70–80.

Jameson, G.B., Anderson, B.F., Norris, G.E., Thomas, D.H., and Baker, E.N. (1998). Structure of human apolactoferrin at 2.0 Å resolution. Refinement and analysis of ligand-induced conformational change. Acta Crystallogr. *D54*, 1319–1335.

Jeffrey, P.D., Bewley, M.C., MacGillivray, R.T., Mason, A.B., Woodworth, R.C., and Baker, E.N. (1998). Ligand-induced conformational change in transferrins: crystal structure of the open form of the N-terminal half-molecule of human transferrin. Biochemistry *37*, 13978–13986.

Jing, S.Q., and Trowbridge, I.S. (1987). Identification of the intermolecular disulfide bonds of the human transferrin receptor and its lipid-attachment site. EMBO J. *6*, 327–331.

Kawabata, H., Yang, S., Hirama, T., Vuong, P.T., Kawano, S., Gombart, A.F., and Koeffler, H.P. (1999). Molecular cloning of transferrin receptor 2 - a new member of the transferrin receptor-like family. J. Biol. Chem. *274*, 20826–20832.

Kretchmar, S.A., and Raymond, K.N. (1988). Effects of ionic strength on iron removal from transferrin. Inorg. Chem. *27*, 1436–1441.

Lawrence, C.M., Ray, S., Babyonyshev, M., Galluser, R., Borhani, D.W., and Harrison, S.C. (1999). Crystal structure of the ectodomain of human transferrin receptor. Science *286*, 779–782.

Lebron, J.A., Bennett, M.J., Vaughn, D.E., Chirino, A.J., Snow, P.M., Mintier, G.A., Feder, J.N., and Bjorkman, P.J. (1998). Crystal structure of the hemochromatosis protein HFE and characterization of its interaction with transferrin receptor. Cell *93*, 111–123.

Lebron, J.A., West, A.P.J., and Bjorkman, P.J. (1999). The hemochromatosis protein HFE competes with transferrin for binding to the transferrin receptor. J. Mol. Biol. *294*, 239–245.

Lim, B.C., McArdle, H.J., and Morgan, E.H. (1987). Transferrin-receptor interaction and iron uptake by reticulocytes of vertebrate animals - a comparative study. J. Comp. Physiol. *B157*, 363–371.

Liu, R., Guan, J.-Q., Zak, O., Aisen, P., and Chance, M.R. (2003). Structural reorganization of transferrin C-lobe and transferrin receptor upon complex formation: C-lobe binds to the receptor helical domain. Biochemistry *42*, 12447–12454.

Mason, A.B., Funk, W.D., MacGillivray, R.T.A., and Woodworth, R.C. (1991). Efficient production and isolation of recombinant amino-terminal half-molecule of human serum transferrin from baby hamster kidney cells. Protein Expr. Purif. *2*, 214–220.

MacGillivray, R.T., Moore, S.A., Chen, J., Anderson, B.F., Baker, H., Luo, Y., Bewley, M., Smith, C.A., Murphy, M.E., Wang, Y., et al. (1998). Two high-resolution crystal structures of the recombinant N-lobe of human transferrin reveal a structural change implicated in iron release. Biochemistry *37*, 7919–7928.

Moody, A.M., Chui, D., Reche, P.A., Priatel, J.J., Marth, J.D., and Reinherz, E.L. (2001). Developmentally regulated glycosylation of the CD8$\alpha\beta$ coreceptor stalk modulates ligand binding. Cell *107*, 501–512.

Nick, H., Acklin, P., Lattmann, R., Buehlmayer, P., Hauffe, S., Schupp, J., and Alberti, D. (2003). Development of tridentate iron chelators: from desferrithiocin to ICL670. Curr. Med. Chem. *10*, 1065–1076.

Qian, Z.M., Li, H., Sun, H., and Ho, K. (2002). Targeted drug delivery via the transferrin receptor-mediated endocytosis pathway. Pharmacol. Rev. *54*, 561–587.

Rao, K., Harford, J.B., Rouault, T., McClelland, A., Ruddle, F.H., and Klausner, R.D. (1986). Transcriptional regulation by iron of the gene for the transferrin receptor. Mol. Cell. Biol. *6*, 236–240.

Rawas, A., Moreton, K., Muirhead, H., and Williams, J. (1989). Preliminary crystallographic studies on duck ovotransferrin. J. Mol. Biol. *208*, 213–214.

Richardson, D.R., and Ponka, P. (1997). The molecular mechanisms of the metabolism and transport of iron in normal and neoplastic cells. Biochim. Biophys. Acta *1331*, 1–40.

Unser, M., Trus, B.L., and Steven, A.C. (1987). A new resolution criterion based on spectral signal-to-noise ratios. Ultramicroscopy *23*, 39–51.

Van Heel, M. (1987). Angular reconstitution: a posteriori assignment of projection directions for 3D reconstruction. Ultramicroscopy *21*, 111–123.

van Heel, M., Harauz, G., Orlova, E.V., Schmidt, R., and Schatz, M. (1996). A new generation of the IMAGIC image processing system. J. Struct. Biol. *116*, 17–24.

West, A.P.J., Giannetti, A.M., Herr, A.B., Bennett, M.J., Nangiana, J.S., Pierce, J.R., Weiner, L.P., Snow, P.M., and Bjorkman, P.J. (2001). Mutational analysis of the transferrin receptor reveals overlapping HFE and transferrin binding sites. J. Mol. Biol. *313*, 385–397.

Wong, J.S., Wang, X., Witte, T., Nie, L., Carvou, N., Kern, P., and Chang, H.C. (2003). Stalk region of beta-chain enhances the co-receptor function of CD8. J. Immunol. *171*, 867–874.

Zak, O., and Aisen, P. (2002). A new method for obtaining human transferrin C-lobe in the native conformation: preparation and properties. Biochemistry *41*, 1647–1653.

Zak, O., and Aisen, P. (2003). Iron release from transferrin, its C-lobe and their complexes with transferrin receptor: the presence of N-lobe accelerates release from C-lobe at endosomal pH. Biochemistry *42*, 12330–12334.

Zak, O., Trinder, D., and Aisen, P. (1994). Primary receptor-recognition site of human transferrin is in the C-terminal lobe. J. Biol. Chem. *269*, 7110–7114.

Zak, O., Tam, B., MacGillivray, R.T.A., and Aisen, P. (1997). A kinetically active site in the C-lobe of human transferrin. Biochemistry *36*, 11036–11043.